Proceedings of ICFDP9:
Ninth International Congress of Fluid Dynamics & Propulsion
December 18-21, 2008, Alexandria, Egypt

ICFDP9-EG-236

FLUTTER BEHAVOIR OF SHAPE MEMORY ALLOY HYBRID COMPOSITE CYLINDRICAL PANELS AT ELEVATED TEMPERATURES

Hesham Hamed Ibrahim
Department of Mechanical Engineering, Hanyang University, Seoul, South Korea.
Space Division, National Authority for Remote Sensing and Space Sciences, Cairo, Egypt.
hesham.ibrahim@narss.sci.eg

Hong Hee Yoo
Department of Mechanical Engineering, Hanyang University, Seoul, South Korea.
hhyoo@hanyang.ac.kr

Kwan-Soo Lee
Department of Mechanical Engineering, Hanyang University, Seoul, South Korea.
ksleehy@hanyang.ac.kr

ABSTRACT

A new nonlinear finite element formulation is presented to predict the thermal buckling and flutter boundaries of shape memory alloy hybrid composite cylindrical panels at elevated temperatures. The governing equations are obtained using Marguerre curved plate theory and the principle of virtual work. The effect of large deflection is included in the formulation through the von Karman nonlinear strain-displacement relations. To account for the temperature dependence of material properties, the thermal strain is stated as an integral quantity of the thermal expansion coefficient with respect to temperature. The aerodynamic pressure is modeled using the quasi-steady first-order piston theory. The Newton-Raphson iteration method is employed to obtain the nonlinear thermal post-buckling deflections, while a frequency domain solution is presented to predict the critical dynamic pressure at elevated temperatures. Numerical results are presented to illustrate the effect of shape memory alloy fiber embeddings, temperature rise, height-to-thickness ratios, and boundary conditions on the panel response.

KEYWORDS:

Flutter boundaries, Thermal buckling, Shape memory alloys, Cylindrical panels.

INTRODUCTION

The external skin of high speed flight vehicles experiences high temperatures due to aerodynamic heating, which can induce thermal buckling and may results in a dynamic instability. In general, thermal buckling does not indicate structural failure. However, large thermal deflections of the skin panels can change its aerodynamic shape affecting reduction in the flight performance. A comprehensive literature review on thermally induced flexure, buckling, and vibration of plates and shells was presented by Tauchart [1] and Thornton [2]. Gray and Mei [3] investigated the thermal post-buckling behavior and free vibration of thermally buckled composite plates using the finite element method. Shi et al. [4] presented a finite element solution for the thermal buckling behavior of laminated composite plates under combined mechanical and thermal loads. Eslami and Javaheri [5] investigated the buckling of composite cylindrical shells under mechanical and thermal loads. The governing equations were derived using Love-Kirchhoff hypothesis and Sander's nonlinear strain-displacement relations. Shen [6] presented a buckling analysis for functionally graded cylindrical thin shells subjected to external pressure and thermal environment. A singular perturbation technique was employed to determine the buckling loads and post-buckling equilibrium paths. Kadoli and Ganesan [7] investigated the linear thermal buckling and free vibration of functionally graded cylindrical shells. First-order shear deformation theories along with Fourier series expansion of the displacement variables were utilized to model the FGM shell.

Panel flutter is a self-excited oscillation of a plate or a shell in supersonic flow. Because of aerodynamic loading on the panel, two eigen modes of the structure merge and lead to this dynamic instability. Panel flutter differs from

wing flutter only in that the aerodynamic force resulting from the air flow acts only on one side of the panel. Ibrahim et al. [8] investigated the thermal buckling and flutter boundaries of thin functionally graded material plates at elevated temperature. They adopted an incremental finite element technique to capture the effect of the temperature-dependence of material properties on the panel response. Ibrahim et al. [9] presented a finite element solution for the thermal buckling and nonlinear flutter performance of thin functionally graded material panels under combined aerodynamic and thermal loads. To account for the temperature-dependence of material properties, the thermal strain was modeled as an integral quantity of thermal expansion coefficient with respect to temperature. Ibrahim et al. [10] extended the formulation presented in [9] by including the shear deformation effect to make it capable of handling thick functionally graded material plates. Singha and Mandal [11] investigated the supersonic flutter boundaries of composite cylindrical shell panels under combined aerodynamic and thermal environments. A 16-noded isoparametric degenerated shell element was employed along with the first-order high Mach number approximation to linear potential flow theory in order to evaluate the aerodynamic pressure. Haddadpour et al. [12] investigated the effect of temperature rise on the flutter boundaries of functionally graded cylindrical shells with simply supported edges. The aeroelastic equations of motion are constructed using Love's shell theory and von Karman–Donnell-type of kinematic nonlinearity coupled with linearized first-order potential (piston) theory.

Shape memory alloys (SMA) have a unique ability to completely recover large pre-strains (up to 10% elongation) when heated above certain characteristic temperature. During the shape recovery process, a large tensile recovery stress occurs if the SMA is restrained. Both the recovery stresses and Young's modules of SMA exhibit highly nonlinear temperature-dependent properties. Birman [12] presented a comprehensive review on the literature concerning SMA up to 1997. Lee et al. [14] investigated the thermal buckling behavior of laminated composite shells with embedded shape memory alloy wires. Modeling and buckling analysis were performed with the use of the ABAQUS code linked with a subroutine for the formulated SMA constitutive equations. Tawfik et al. [15] proposed a novel concept in enhancing the thermal buckling and aeroelastic behavior of plates through embedding SMA fibers in it. Park et al. [16] investigated the nonlinear vibration behavior of thermally buckled composite plates embedded with shape memory alloy fibers. An incremental method was adopted to account for the temperature dependent material properties. Roh et al. [17] investigated the thermal post-buckling response of shape memory alloy hybrid composite shell panels. The layer-wise displacement theory and the cylindrical arc length method were utilized in the formulation. Ibrahim et al. [18] investigated the thermal buckling and free vibration behavior of thick, shape memory alloy hybrid composite plates. Moreover, a frequency domain solution for predicting panel flutter boundaries at elevated temperatures was presented. Ibrahim et al. [19] investigated the nonlinear random response of moderately thick composite plates impregnated with pre-strained shape memory alloy fibers under combined thermal and random acoustic loads. Ibrahim et al. [20] presented a new nonlinear finite element formulation to predict the aero-thermal deflection and fundamental frequencies of SMA hybrid composite panels with initial sinusoidal geometric imperfection.

This paper is an extension of the work presented in [18] and [20] by presenting a frequency domain solution to predict the flutter boundaries of shape memory alloy hybrid composite shallow cylindrical panels at elevated temperatures. In this work, a new nonlinear finite element model is presented for the prediction of thermal post-buckling equilibrium paths and flutter critical dynamic pressures of a shape memory alloy hybrid composite (SMAHC) cylindrical panel under combined thermal and aerodynamic loads. The nonlinear governing equations for a thin, cylindrical rectangular panel are obtained using Marguerre curved plate theory, von Karman strain-displacement relations, and the principle of virtual work. To account for the temperature-dependence of material properties, the thermal strain is modeled as an integral quantity of the thermal expansion coefficient with respect to temperature [9]. Numerical results are provided to show the effect of the temperature rise, pre-strained SMA fiber embeddings, height-to-thickness ratios and boundary conditions on the panel response.

FINITE ELEMENT FORMULATION

Nonlinear Strain-Displacement Relations

The nodal degrees of freedom vector $\{\theta\}$ of a rectangular four-nodded Bogner-Fox-Schmidt (BFS) C^1 conforming plate element having 6 degrees of freedom at each node can be written as:

$$\{\theta\} = \left\{ \left\{ w, \frac{\partial w}{\partial x}, \frac{\partial w}{\partial y}, \frac{\partial^2 w}{\partial x \partial y} \right\}, \{u, v\} \right\}^T = \begin{Bmatrix} \{w_b\} \\ \{w_m\} \end{Bmatrix} \tag{1}$$

where $\{w_b\}$ is the nodal transverse displacement and rotations vector and $\{w_m\}$ is the nodal membrane displacements vector. Consider the cylindrical panel surface w_o and the lateral deflection w shown in Fig. 1, the Marguerre curved plate strain-displacement relation along with von Karman large deflection can be written as [21]:

$$\begin{Bmatrix}\varepsilon_x\\ \varepsilon_y\\ \gamma_{xy}\end{Bmatrix}=\begin{Bmatrix}\frac{\partial u}{\partial x}\\ \frac{\partial v}{\partial y}\\ \frac{\partial u}{\partial y}+\frac{\partial v}{\partial x}\end{Bmatrix}+\begin{Bmatrix}\frac{1}{2}\left(\frac{\partial w}{\partial x}\right)^2\\ \frac{1}{2}\left(\frac{\partial w}{\partial y}\right)^2\\ \frac{\partial w}{\partial x}\frac{\partial w}{\partial y}\end{Bmatrix}+\begin{Bmatrix}\frac{\partial w}{\partial x}\frac{\partial w_o}{\partial x}\\ \frac{\partial w}{\partial y}\frac{\partial w_o}{\partial y}\\ \frac{\partial w}{\partial x}\frac{\partial w_o}{\partial y}+\frac{\partial w_o}{\partial x}\frac{\partial w}{\partial y}\end{Bmatrix}+z\begin{Bmatrix}-\frac{\partial^2 w}{\partial x^2}\\ -\frac{\partial^2 w}{\partial y^2}\\ -2\frac{\partial^2 w}{\partial x\partial y}\end{Bmatrix} \quad (2)$$

Or in a compact form as:

$$\{\varepsilon\}=\{\varepsilon_m^o\}+\{\varepsilon_b^o\}+\{\varepsilon_{wo}^o\}+z\{\kappa\} \quad (3)$$

$\{\varepsilon_m^o\}$, $\{\varepsilon_b^o\}$, $\{\varepsilon_{wo}^o\}$, and $z\{\kappa\}$ are the membrane linear strain vector, the membrane nonlinear strain vector, inplane strain vector due to panel curvature and the bending strain vector, respectively. In addition, the cylindrical panel adopted in this study is assumed to have a constant radius in the *x*-direction and an infinite radius in the *y*-direction, and the cylindrical curved surface $w_o(x)$ may be approximated by the following form [21]:

$$w_o(x)=H\left(1-\frac{(x-(a/2))^2}{(a/2)^2}\right) \quad (4)$$

where *H* is the maximum height-rise and *a* are the panel dimension along the *x*-direction.

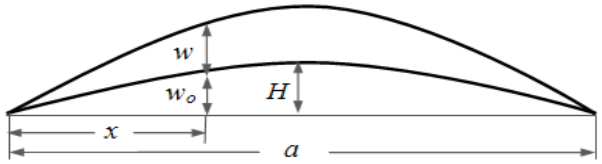

Figure 1. Schematic for the initial cylindrical surface w_o and the transverse deflection *w*

Constitutive Equations

For the k[th] composite lamina impregnated with SMA fibers, the stress-strain relations can be expressed as [19]:

$$\begin{Bmatrix}\sigma_x^k\\ \sigma_y^k\\ \tau_{xy}^k\end{Bmatrix}=\left[\overline{Q}^k(T)\right]\{\varepsilon\}+V_s^k\{\sigma_r^k(T)\}-V_m^k\int_{T_{ref}}^{T}\left[\overline{Q}_m^k(\tau)\right]\{\alpha_m^k(\tau)\}d\tau \quad (5)$$

where $\{\sigma\}$ and $\{\sigma_r\}$ are the inplane and the SMA recovery stress vectors at a given temperature *T*. V_m and V_s are the volume fractions of the composite matrix and SMA fibers, respectively. In addition, $\{\alpha_m\}$, $[\overline{Q}]$ and $[\overline{Q}_m]$ are the thermal expansion coefficient vector of the composite matrix, the transformed reduced stiffness matrix of the SMAHC lamina, and the transformed reduced stiffness matrix of the composite matrix, respectively. Note that the SMA fibers are embedded in same direction of the composite matrix fibers, and assumed uniformly distributed within each layer. Integrating Eq.5 over the plate thickness *h*, the constitutive equation is obtained as:

$$\begin{Bmatrix}\{N\}\\ \{M\}\end{Bmatrix}=\begin{bmatrix}[A] & [B]\\ [B] & [D]\end{bmatrix}\begin{Bmatrix}\{\varepsilon_m^o\}+\{\varepsilon_b^o\}+\{\varepsilon_{wo}^o\}\\ \{\kappa\}\end{Bmatrix}-\begin{Bmatrix}\{N_T\}\\ \{M_T\}\end{Bmatrix}+\begin{Bmatrix}\{N_r\}\\ \{M_r\}\end{Bmatrix} \quad (6)$$

where

$$\begin{Bmatrix}N_T\\ M_T\end{Bmatrix}=V_m\int_{-h/2}^{h/2}\left[\left(\int_{T_{ref}}^{T}[Q_m(\tau)]\{\alpha_m(\tau)\}d\tau\right)\right]\begin{Bmatrix}1\\ z\end{Bmatrix}dz,$$

$$\begin{Bmatrix}N_r\\ M_r\end{Bmatrix}=V_s\int_{-h/2}^{h/2}\{\sigma_r\}\begin{Bmatrix}1\\ z\end{Bmatrix}dz$$

Aerodynamic Pressure Loading

The first-order quasi-steady piston theory for supersonic flow states that [15]:

$$P_a=-\left(\frac{g_a}{\omega_o}\frac{D_{110}}{a^4}\frac{\partial(w+w_o)}{\partial t}+\lambda\frac{D_{110}}{a^3}\frac{\partial(w+w_o)}{\partial x}\right) \quad (7)$$

with,

$$g_a=\frac{\rho_a v(M_\infty^2-2)}{\rho h\omega_o\beta^3}=\sqrt{\lambda C_a},\quad C_a=\frac{(M_\infty^2-2)^2}{(M_\infty^2-1)^2}\frac{\rho_a a}{\rho h\beta},\quad \lambda=\frac{2qa^3}{\beta D_{11O}},$$

$$q=\frac{\rho_a v^2}{2},\quad \beta=\sqrt{M_\infty^2-1},\quad and\quad \omega_o=\left(\frac{D_{11O}}{\rho h a^4}\right)^{\frac{1}{2}}$$

where P_a is the aerodynamic pressure loading, *v* is the airflow velocity on one side of the panel, M_∞ is the Mach number, *q* is the dynamic pressure, ρ_a is the air mass density, g_a is the non-dimensional aerodynamic damping, C_a is the aerodynamic damping coefficient, λ is the non-dimensional dynamic pressure, D_{110} is the first entry in the flexural stiffness matrix *D* (1, 1) when all the fibers of the composite layers are aligned in the airflow *x*-direction, and a is the stream wise panel length.

Governing Equations

The principle of virtual work states that:

$$\delta Work=\delta Work_{int}-\delta Work_{ext}=0 \quad (8)$$

where the virtual work done by internal stresses can be written as:

$$\begin{aligned}\delta Work_{int}&=\int_A\begin{pmatrix}\{\delta(\{\varepsilon_m^o\}+\{\varepsilon_b^o\}+\{\varepsilon_{wo}^o\})\}^T\{N\}\\ +\{\delta\kappa\}^T\{M\}\end{pmatrix}dA\\ &=\{\delta\theta\}^T\begin{pmatrix}[k]+[k_{wo}]-[k_T]+[k_r]\\ +\frac{1}{2}([n1]+[n1_{wo}])+\frac{1}{3}[n2]\end{pmatrix}\{\theta\}\\ &\quad-\{\delta\theta\}^T(\{p_T\}+\{p_{Two}\}-\{p_r\}-\{p_{rwo}\})\end{aligned} \quad (9)$$

where $[k]$, $[k_T]$ and $[k_r]$ are the linear, thermal and recovery stress stiffness matrices; $[k_{wo}]$ is a linear stiffness matrix due to initial cylindrical panel geometry w_o; $[n1]$ and $[n2]$ are the first- and second-order nonlinear stiffness matrices, respectively; $[n1_{wo}]$ is a first-order stiffness matrix due to cylindrical panel geometry. In addition, $\{p_T\}$ and $\{p_r\}$ are thermal and recovery stress load vectors, and $\{p_{Two}\}$ and $\{p_{rwo}\}$ are thermal and recovery load vectors due to cylindrical panel geometry. On the other hand, the external virtual work $\delta Work_{ext}$ can be stated as follows [9]:

$$\begin{aligned}\delta Work_{ext} &= \int_A \begin{pmatrix} \delta w\left(-\rho h\frac{\partial^2 w}{\partial t^2}+P_a\right)+\delta u\left(-\rho h\frac{\partial^2 u}{\partial t^2}\right) \\ +\delta v\left(-\rho h\frac{\partial^2 v}{\partial t^2}\right)\end{pmatrix} dA \\ &= -\{\delta\theta\}^T[m]\{\ddot{\theta}\}-\{\delta\theta\}^T[g]\{\dot{\theta}\}-\{\delta\theta\}^T\lambda[a_a]\{\theta\} \\ &\quad -\{\delta\theta\}^T\lambda\{p^{sal}\}\end{aligned} \tag{10}$$

where $[m]$, $[g]$ and $[a]$ are mass, aerodynamic damping, and aerodynamic stiffness matrices, respectively. $\{p^{sal}\}$ is a static aerodynamic load vector which is function of the initial cylindrical panel geometry w_o. By substituting Eqs.9 and 10 into 8, the governing equations for a shape memory alloy hybrid composite cylindrical panel under the combined action of thermal and aerodynamic loads, can be written as:

$$\begin{aligned}[M]\{\ddot{W}\}+[G]\{\dot{W}\}+\begin{pmatrix}\lambda[A_a]+[K]+[K_{wo}]-[K_T] \\ +[K_r]+\frac{1}{2}([N1]+[N1_{wo}])+\frac{1}{3}[N2]\end{pmatrix}\{W\} \\ =\{P_T\}+\{P_{Two}\}-\{P_r\}-\{P_{rwo}\}-\lambda\{P^{sal}\}\end{aligned} \tag{11}$$

SOLUTION PROCEDURES

The solution of the system of ordinary differential equations presented in Eq.11 can be separated as the sum of a time-independent particular solution and a time-dependent homogenous solution. The total deflection can be written as:

$$\{W\}=\{W\}_s+\{W\}_t \tag{12}$$

The particular solution characterizes a static thermal post-buckling deflection $\{W\}_s$, while the homogenous solution characterizes a self-exited dynamic flutter oscillation $\{W\}_t$ about the static equilibrium position $\{W\}_s$. Substituting Eq. 12 into 11 results in the following:

$$\begin{aligned}[M]\{\ddot{W}\}_t+[G]\{\dot{W}\}_t+\begin{pmatrix}\lambda[A_a]+[K]+[K_{wo}] \\ -[K_T]+[K_r]+\frac{1}{2}([N1]_{s+t}) \\ +\frac{1}{2}[N1_{wo}]_{s+t}+\frac{1}{3}[N2]_{s+t}\end{pmatrix}(\{W\}_s+\{W\}_t) \\ =\{P_T\}+\{P_{Two}\}-\{P_r\}-\{P_{rwo}\}-\lambda\{P^{sal}\}\end{aligned} \tag{13}$$

where the subscript (s + t) denotes that the corresponding nonlinear stiffness matrix is evaluated using the total deflection. Equation 13 can be separated into static and dynamic equations as follows [10]:

$$\begin{aligned}&\begin{pmatrix}\lambda[A_a]+[K]+[K_{wo}]-[K_T]+[K_r] \\ +\frac{1}{2}([N1]_s+[N1_{wo}]_s)+\frac{1}{3}[N2]_s\end{pmatrix}\{W\}_s \\ &=\{P_T\}+\{P_{Two}\}-\{P_r\}-\{P_{rwo}\}-\lambda\{P^{sal}\}\end{aligned} \tag{14}$$

$$\begin{aligned}&[M]\{\ddot{W}\}_t+[G]\{\dot{W}\}_t+\begin{pmatrix}\lambda[A_a]+[K]+[K_{wo}] \\ -[K_T]+[K_r]+\frac{1}{2}([N1]_t) \\ +\frac{1}{2}[N1_{wo}]_t+\frac{1}{3}[N2]_t\end{pmatrix}\{W\}_t \\ &+([N1]_s+[N1_{wo}]_s+[N2]_s+[N2]_{st})\{W\}_t=\{0\}\end{aligned} \tag{15}$$

Thermal Post-Buckling Deflection

For the thermal post-buckling problem, the solution procedure using Newton-Raphson iteration method is presented in the following. Introducing the function $\{\Psi(W)\}$ to Eq.14 to be:

$$\begin{aligned}\{\Psi(W_s)\}&=\begin{pmatrix}\lambda[A_a]+[K]+[K_{wo}]-[K_T]+[K_r] \\ +\frac{1}{2}([N1]_s+[N1_{wo}]_s)+\frac{1}{3}[N2]_s\end{pmatrix}\{W\}_s \\ &\quad -\{P_T\}-\{P_{Two}\}+\{P_r\}+\{P_{rwo}\}+\lambda\{P^{sal}\}=0\end{aligned} \tag{16}$$

Equation 16 can be written in the form of a truncated Taylor series as:

$$\{\Psi(W_s+\delta W)\}=\{\Psi(W_s)\}+\frac{d\{\Psi(W_s)\}}{d(W_s)}\{\delta W\}\cong 0 \tag{17}$$

where [10],

$$\begin{aligned}\frac{d\{\Psi(W_s)\}}{d(W_s)}&=\begin{pmatrix}\lambda[A_a]+[K]+[K_{wo}]-[K_T]+ \\ [K_r]+[N1]_s+[N1_{wo}]_s+[N2]_s\end{pmatrix} \\ &=[K_{tan}]\end{aligned} \tag{18}$$

Thus, the Newton-Raphson iteration procedure for the determination of the thermal post-buckling deflection can be expressed as follows:

$$\{\Psi(W_s)\}_i = \begin{pmatrix} \lambda[A_a]+[K]+[K_{wo}]-[K_T]+[K_r] \\ +\frac{1}{2}([N1]_s+[N1_{wo}]_s)_i+\frac{1}{3}([N2]_s)_i \end{pmatrix}(\{W\}_s)_i \\ -\{P_T\}-\{P_{Two}\}+\{P_r\}+\{P_{rwo}\}+\lambda\{P^{sal}\}$$

$$[K_{\tan}]_i\{\delta W\}_{i+1} = -\{\Psi(W_s)\}_i$$

$$\{\delta W\}_{i+1} = -[K_{\tan}]^{-1}\{\Psi(W_s)\}_i$$

$$\{W_s\}_{i+1} = \{W_s\}_i + \{\delta W\}_{i+1}$$

Convergence occurs in the above procedure when the maximum value of $\{\delta W\}_{i+1}$ becomes less than a given tolerance ε_{tol}, i.e. max $|\{\delta W\}_{i+1}| \le \varepsilon_{tol}$.

Flutter Boundaries at Elevated Temperatures

In this section, the procedure of determining the critical non-dimensional dynamic pressure at elevated temperatures is presented. By assuming $\{W\}_t << 1$, all the dynamic nonlinear terms will be dropped from Eq.15 and the linearized dynamic equation of motion which represents the flutter boundary at elevated temperatures can be stated as follows:

$$[M]\{\ddot{W}\}_t + [G]\{\dot{W}\}_t + \begin{pmatrix} \lambda[A_a]+[K]+[K_{wo}] \\ -[K_T]+[K_r]+[N1]_s \\ +[N1_{wo}]_s+[N2]_s \end{pmatrix}\{W\}_t = \{0\} \quad (19)$$

Or

$$\begin{bmatrix} M_b & 0 \\ 0 & M_m \end{bmatrix}\begin{Bmatrix} \ddot{W}_b \\ \ddot{W}_m \end{Bmatrix} + \begin{bmatrix} G_b & 0 \\ 0 & 0 \end{bmatrix}\begin{Bmatrix} \dot{W}_b \\ \dot{W}_m \end{Bmatrix} \\ + \begin{pmatrix} \lambda\begin{bmatrix} A_{ab} & 0 \\ 0 & 0 \end{bmatrix}+\begin{bmatrix} K_b & K_{bm} \\ K_{mb} & K_m \end{bmatrix}+\begin{bmatrix} K_{wob} & K_{wobm} \\ K_{womb} & 0 \end{bmatrix} \\ -\begin{bmatrix} K_{Tb} & 0 \\ 0 & 0 \end{bmatrix}+\begin{bmatrix} K_{rb} & 0 \\ 0 & 0 \end{bmatrix} \\ +\begin{bmatrix} N1_b+N1_{wob} & N1_{bm} \\ N1_{mb} & 0 \end{bmatrix}_s+\begin{bmatrix} N2_b & 0 \\ 0 & 0 \end{bmatrix}_{ss} \end{pmatrix}\begin{Bmatrix} W_b \\ W_m \end{Bmatrix} = \begin{Bmatrix} 0 \\ 0 \end{Bmatrix} \quad (20)$$

Neglecting the in-plane inertia term will not bring significant error, because their natural frequencies are usually 2 to 3 orders of magnitude higher than the bending ones [19]. Therefore, for a SMAHC cylindrical panel with symmetric lamination, the linearized transverse dynamic equation can be stated as:

$$[M_b]\{\ddot{W}_b\}_t + [G_b]\{\dot{W}_b\}_t + \begin{pmatrix} \lambda[A_{ab}]+[K_b]+[K_{wo_b}] \\ -[K_{Tb}]+[K_{rb}] \\ +[N1_b+N1_{wob}]_s+[N2_b]_s \end{pmatrix}\{W_b\}_t = \{0\} \quad (21)$$

Now, assuming the deflection function of the transverse displacement $\{W_b\}_t$ to be in the form,

$$\{W_b\}_t = \bar{c}\{\Phi_b\}e^{\Omega t} \quad (22)$$

where $\Omega = \alpha + i\omega$ is the complex panel motion parameter (α is the damping ratio and ω is the frequency), $\bar{c}$ is the amplitude of vibration, and $\{\Phi_b\}$ is the mode shape. Substituting Eq. 22 into 21, the generalized eigenvalue problem can be stated as,

$$\bar{c}\left[\kappa[M]+\left[\overline{K}\right]\right]\{\Phi_b\}e^{\Omega t} = \{0\} \quad (23)$$

where

$$\kappa = \Omega^2 + \omega_o g_a \Omega$$

$$\left[\overline{K}\right] = \begin{pmatrix} \lambda[A_{ab}]+[K_b]+[K_{wo_b}]-[K_{Tb}] \\ +[K_{rb}]+[N1_b+N1_{wob}]_s+[N2_b]_s \end{pmatrix}$$

From Eq. 23, we can write the generalized eigenvalue problem as:

$$\left[-\kappa[M_b]+\left[\overline{K}\right]\right]\{\Phi_b\} = \{0\} \quad (24)$$

where κ is the eigenvalue and Φ_b is the mode shape vectors of the following characteristic equation:

$$\left|-\kappa[M_b]+\left[\overline{K}\right]\right| = \{0\} \quad (25)$$

Given that the values of κ are real for all values of λ below the critical value, an iterative solution can be utilized to determine the value of the critical non-dimensional dynamic pressure λ_{cr}.

NUMERICAL RESULTS AND DISCUSSIONS

This section presents numerical results for the thermal post-buckling deflections and the flutter boundaries at elevated temperatures of a laminated composite cylindrical panel with and without SMA fibers. Convergence was found to occur at a uniform 8 x 8 finite element mesh of a rectangular four-nodded Bogner-Fox-Schmidt (BFS) C^1 conforming plate element and thus used. The dimensions of the composite cylindrical panel adopted throughout this study are 0.381 x 0.305 x 0.0013 (m) and the stacking sequence is $[0/-45/45/90]_s$. the four edges of the panel will be all simply supported or all clamped. Table (1) presents the material properties of both composite matrix and SMA fibers [19], while the variation of the modulus of elasticity and recovery stress of a trained SMA fibers, made from Nitinol, are presented in Figs. 2 and 3 [22]. Uniform temperature change was applied to the plate, and the reference temperature is assumed to be 21ºC.

Table1 Material properties for both of the composite matrix and the Nitinol fibers

Nitinol	Graphite-epoxy

See Figs. 2 and 3 for Young's modulus and recovery stresses.	**E1** 155 (1-6.35x10^{-4} ΔT) GPa **E2** 8.07 (1-7.69x10^{-4} ΔT) GPa
G 25.6 GPa	**G12** 4.55(1-1.09x10^{-3}ΔT) GPa
ρ 6450 Kg/m^3	**ρ** 1550 Kg/m^3
ν 0.3	**ν** 0.22
α 10.26 x 10^{-6} / ºC	**α1** -0.07x10^{-6}(1-0.69x10^{-3}ΔT) / ºC **α2** 30.6x10^{-6}(1+0.28x10^{-4}ΔT) / ºC

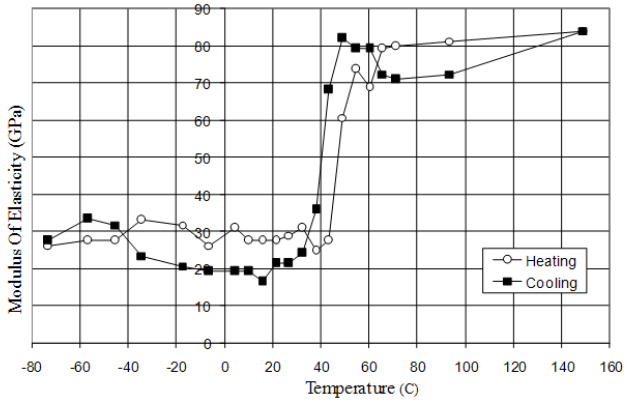

Figure 2 Modulus of elasticity variation with temperature for a trained Nitinol fiber

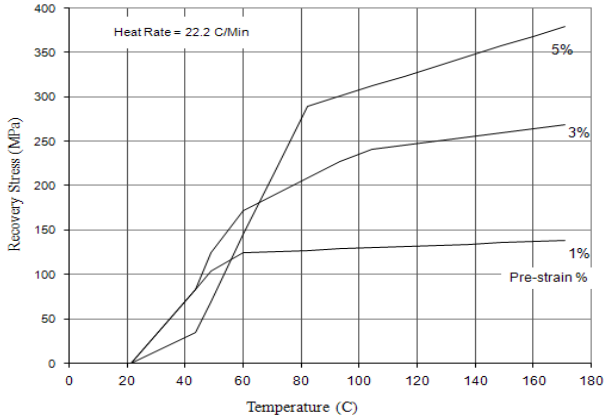

Figure 3 Nitinol recovery stress as a function of both temperature and pre-strain percentage

Figures 4 and 5 present the thermal post-buckling equilibrium paths for a simply supported cylindrical composite panel illustrating the effect of both SMA fiber embeddings and height to thickness ratio (*H/h*). Figure 4 presents the thermal buckling of a simply supported cylindrical composite panel with different height to thickness ratio. It is seen that increasing *H/h* value has a noticeable effect on the panel response through decreasing the post-buckling deflection especially at high temperatures. It is also seen that, the clamped composite plate is more thermally stable than the simply supported one. But at high temperatures, both plates have almost the same post-buckling deflections. Because, in simply supported plates, the nonlinear stiffness terms build up faster than those of the clamped plate which compensates the lower thermal stability of simply supported plate panels.

Figure 5 presents the thermal buckling of a simply supported SMAHC cylindrical panel with 5% SMA volume fraction and a pre-strain of 5%. It is seen that SMA fiber embeddings result in increasing the buckling temperature and decreasing, or suppressing the post-buckling deflection.

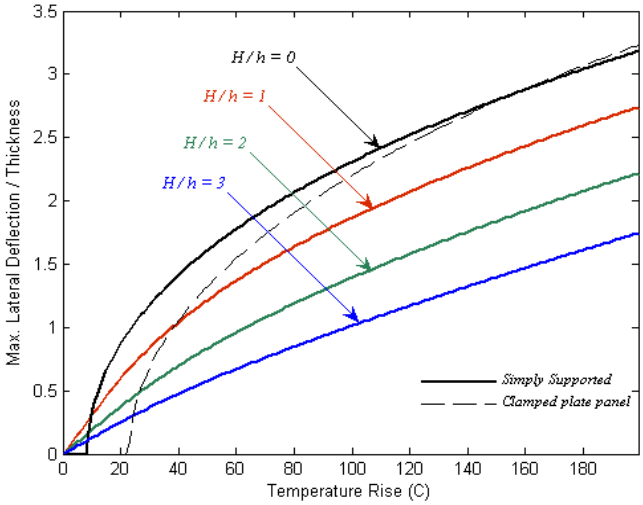

Figure 4 Maximum non-dimensional thermal deflection of a simply supported composite cylindrical panel with different height to thickness ratios (*H/h*)

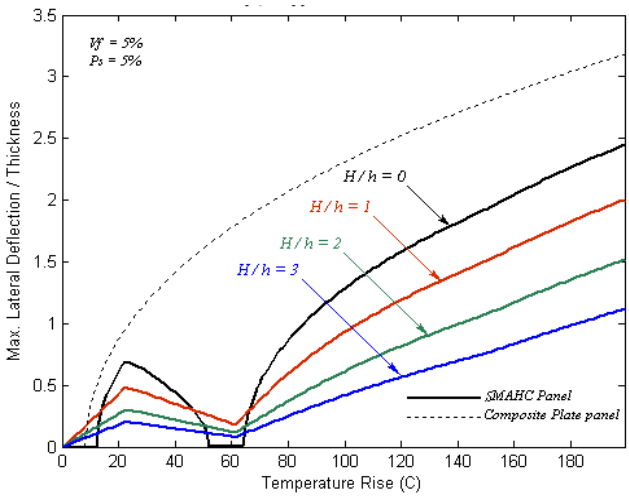

Figure 5 Maximum non-dimensional thermal deflection of a simply supported SMAHC cylindrical panel with different height to thickness ratios (*H/h*)

It is also seen that, the SMAHC plate panel (*H/h* = 0) has two buckling temperatures. This is because for the temperature range from 21 to 43ºC, the 5% pre-stain curve, shown in Fig. 3, has a slower rate of recovery-stress increase with temperature than that of the 1% and 3% pre-

strains, which makes the thermal stress dominates the SMA recovery stress during this temperature range, and hence, the plate experiences thermal buckling. But for temperatures above 43ºC, the 5% pre-stain curve has a higher rate of increase than that of temperatures lower than 43ºC, which causes the recovery stress to dominate the thermal stress, compensating the former low recovery stresses by making the plate goes flat again at 72ºC (i.e. at a temperature rise = 51ºC), before reaching the second thermal buckling point at 86ºC. That is why the performance of the 5% pre-strain is always lower than that of the 1% and 3% pre-strain values in the temperature range from 21 to 43ºC, i.e., from room temperature up to a temperature rise of 22ºC. It is also found that the cylindrical panel response is superior compared to that of the plate panel except at temperature rises from 51ºC up to 65ºC.

For the clamped composite panels presented in Fig. 6, it is seen that, for all cylindrical panels, there is no sudden out-of-plane deflection, i.e. buckling phenomenon, because any small temperature rise results in a prompt transverse deflection of the panel due to the initial curvature of the panel, that makes all curved panels lose their distinct critical buckling temperature. It is also seen that the cylindrical panels have superior performance at elevated temperatures except at the temperature rises less than 21.5 ºC, i.e. before the buckling point of the clamped composite plate panel.

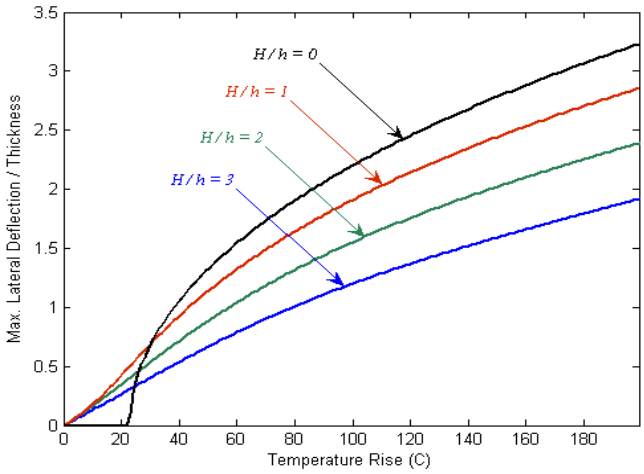

Figure 6 Maximum non-dimensional thermal deflection of a clamped composite cylindrical panel with different height to thickness ratio (*H/h*)

Figure 7 presents the thermal post-buckling deflections for a clamped SMAHC panel with 5% SMA volume fraction and a pre-strain of 5%. It is seen that the presence of multiple buckling points, as was the case in the simply supported SMAHC plate panel, has been completely hindered by clamping the plate edges. It is also found that the SMAHC plate panel (*H/h* = 0) has superior performance up to a temperature rise of 84ºC compared to those of the cylindrical panels. Figure 8 presents a comparison between the flutter boundaries of simply supported and clamped composite panels. The results reveal that the clamped edges are not always favorable regarding flutter stability at elevated temperatures. Because of the early thermal buckling of the simply supported composite plate panel, compared to the clamped one, the nonlinear stiffness added the system, due to thermal deflection, compensates the low flutter stability of the simply supported plate at low temperatures. But, it is going to be a matter of compromise between two situations; first, having thermally buckled plate with higher flutter boundaries at elevated temperatures, resulting in a change in the aerodynamic shape and hence deteriorating the flight performance, which is the case in simply supported plate panels; second, having better thermal static stability at elevated temperatures along with lower critical dynamic pressures λ, which is the case in clamped plate panels. It is also found that cylindrical panels always have superior dynamic stability compared to plate panels. Moreover, by increasing the height to thickness ratio (*H/h*), the panel dynamic stability becomes less sensitive to temperature rise.

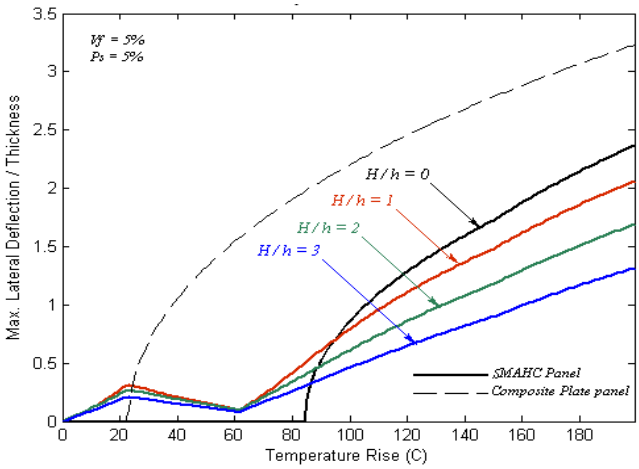

Figure 7 Maximum non-dimensional thermal deflection of a clamped SMAHC cylindrical panel with different height to thickness ratios (*H/h*)

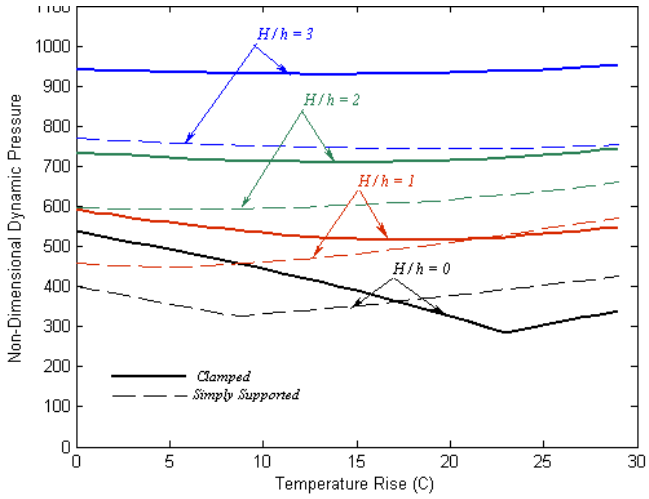

Figure 8 Flutter boundaries of simply supported and clamped composite cylindrical panels with different height to thickness ratio (*H/h*)

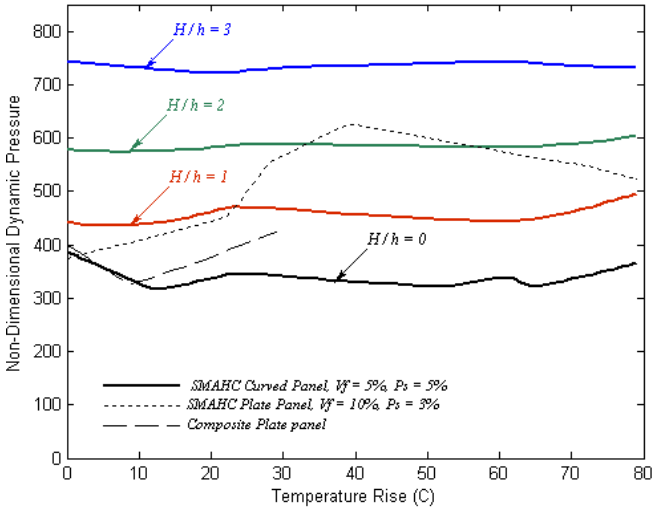

Figure 9 Flutter boundaries of simply supported SMAHC cylindrical panels with different height to thickness ratio (*H/h*)

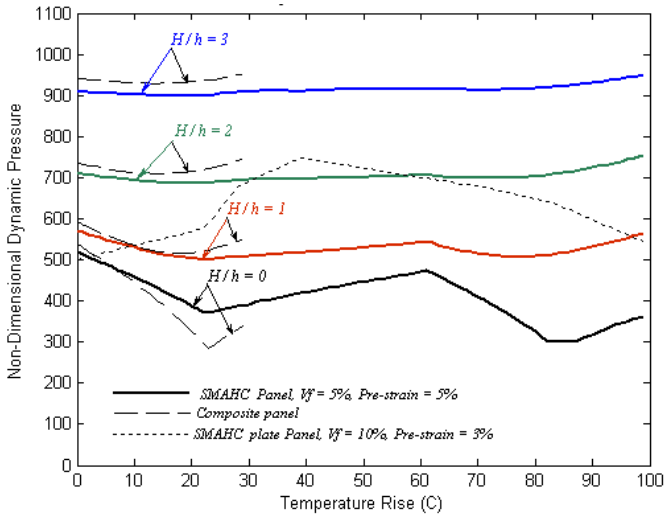

Figure 10 Flutter boundaries of clamped SMAHC cylindrical panels with different height to thickness ratio (*H/h*)

Figures 9 and 10 present the critical non-dimensional dynamic pressure versus temperature curves for different SMA volume fractions, pre-strains, and height to thickness ratios for both simply supported and clamped edges. Figure 3 shows that, in the temperature rise range 21-43ºC, the 5% pre-stain curve has a slower rate of recovery-stress rise with temperature than that of the 3% pre-strain. This makes the thermal stress dominates the SMA recovery stress during this temperature range, and hence, the critical dynamic pressure decreases steeply with temperature rise, until the occurrence of buckling, compared to the 3% pre-strain curve shown in Fig 9. It is also seen that the composite panel curves seize to increase at much lower temperatures compared to those of the SMAHC panels. Because, at temperatures slightly higher than the critical buckling temperature, the panel is most likely to undergo chaotic limit-cycle oscillations. Therefore, the SMAHC panels are always having superior dynamic stability compared to the composite panels, since it can survive much higher temperatures without the occurrence of flutter chaotic oscillations along with noticeably increase the flutter critical dynamic pressures compared to the composite panels. For the clamped SMAHC plate panel seen in Fig.10, it is found the flutter boundary for the 5% pre-strain value is more sensitive to temperature rise than that of the simply supported plate. Because, the earlier thermal deflection of the simply supported plate added nonlinear stiffness to the system which compensates the decreased stiffness due to temperature rise.

CONCLUSTIONS

A new nonlinear finite element formulation is presented to predict the thermal buckling and flutter boundaries of shape memory alloy hybrid composite cylindrical panels at elevated temperatures. The governing equations are obtained using Marguerre curved plate theory and the principle of virtual work. The effect of large deflection is included in the formulation through the von Karman nonlinear strain-displacement relations. The temperature dependence of material properties for the composite matrix and *SMA* fibers is considered in the formulation. The Newton-Raphson iteration method is employed to obtain the nonlinear deflections, while an Eigen value problem is solved at each temperature rise to predict the flutter critical

dynamic pressure. Results showed that the clamped composite plate panel is more thermally stable than the simply supported one. But at high temperatures, both plates have almost the same post-buckling deflections. Because, in simply supported plate panels, the nonlinear stiffness terms build up faster than those of the clamped plate which compensates the lower thermal stability of simply supported plate panels. It was also found that, the cylindrical panels are not always having superior performance than the plate panels regarding thermal buckling. The results revealed that the clamped edges are not always favorable regarding flutter stability at elevated temperatures. But, it is going to be a matter of compromise between two situations; first, having thermally buckled plate with higher flutter boundaries at elevated temperatures, resulting in a change in the aerodynamic shape and hence deteriorating the flight performance, which is the case in simply supported plate panels; second, having better thermal static stability at elevated temperatures along with lower critical dynamic pressures λ and hence a fatigue problem, which is the case in clamped plate panels. Finally, it is found that the SMA fiber embeddings can be very useful in controlling the plate static thermal response through increasing the buckling temperature and decreasing or suppressing the thermal post-buckling deflections. Moreover, the SMAHC panels are efficient in controlling flutter by highly increasing the flutter boundaries at elevated temperatures compared to those of the composite panels.

NOMENCLATURE

[A], [B], [D]	In-plane, coupling, and bending matrices of a laminate
$[A_a]$	Aerodynamic stiffness matrix
[G]	Aerodynamic damping matrix
[K], [M]	System linear stiffness and mass matrices
$[K_{tan}]$	System tangent stiffness matrix
{N}, {M}	Force and moment resultant vectors
[N1], [N2]	System first- and second-order nonlinear stiffness matrices
$[\overline{Q}]$	Transformed lamina reduced stiffness matrix
T_{ref}	Reference temperature
V_s, V_m	Volume fractions of the SMA fibers and the composite matrix
{W}	System nodal displacement vector
α	Thermal expansion coefficient
λ	Non-dimensional dynamic pressure
σ_r	Nitinol fibers recovery stress
h	Thickness
H	Maximum height-rise

Subscripts

b	Bending
i	Iteration number
m	Membrane or composite matrix
r	Due to recovery stress of Nitinol fibers
s	Static or quantity related to SMA fibers
st	Dependent on both static and dynamic displacements
t	Dynamic or time dependent
x, y, z	Plate Cartesian coordinates

ACKNOWLEDGMENTS

This work was supported by the BK21 program, Hanyang University, Seoul, South Korea. The authors wish to express their gratitude for this financial support.

REFERENCES

[1] T. R. Tauchart, "Thermally Induced Flexure, Buckling, and Vibration of Plates", *Appl. Mech. Rev.*, Vol. 44, No. 8, pp. 347-360, 1991.

[2] E. A. Thornton, "Thermal Buckling of Plates and Shells", *Appl. Mech. Rev.*, Vol. 46, No. 10, pp. 485-506, 1993.

[3] Gray, C.C., and Mei, C., "Finite Element Analysis of Thermal Postbuckling and Vibrations of Thermally Buckled Composite Plates, proceedings of the *32nd AIAA/ASME/ASCE/ AHS/ASC Structures, Structural Dynamics, and Materials Conference*, Pt. 4, AIAA, Washington, DC, pp. 2996–3007, 1991.

[4] Y. Shi, R. Y. Lee, and C. Mei, "Coexiting Thermal Post-Buckling Of Composite Plates With Initial Imperfections Using Finite Element Modal Method", *Journal of Thermal Stresses*, Vol. 22, pp. 595-614, (1999).

[5] M. R. Eslami and R. Javaheri, "Buckling of Composite Cylindrical Shells under Mechanical and Thermal Loads", *Journal of Thermal Stresses*, Vol. 22, pp. 527-545, 1999.

[6] Hui-Shen Shen, "Postbuckling Analysis of Pressure-Loaded Functionally Graded Cylindrical Shells in Thermal Environments", *Engineering Structures*, Vol. 25, pp. 487-497, 2003.

[7] R. Kadoli, and N. Ganesan, "Buckling and Free Vibration Analysis of Functionally Graded Cylindrical Shells Subjected to a Temperature-Specified Boundary Condition", *Journal of Sound and Vibration*, Vol. 289, pp. 450-480, 2006.

[8] H. H. Ibrahim, M. Tawfik, and M. Al-Ajmi, "Aero-Thermo-Mechanical Characteristics of Functionally Graded Material Panels with Temperature-Dependent Material Properties," Proceedings of the *8th International Congress of Fluid Dynamics and Propulsion (ICFDP 8)*, *ASME* Paper ICFDP-EG-116, 2006.

[9] H. H. Ibrahim, M. Tawfik, and M. Al-Ajmi, "Non-Linear Panel Flutter for Temperature-Dependent Functionally Graded Material Panels", *Computational Mechanics*, Vol. 41, No. 2, pp. 325–334, 2007.

[10] H. H. Ibrahim, M. Tawfik, and M. Al-Ajmi, "Thermal Buckling and Nonlinear Flutter Behavior of

Functionally Graded Material Panels," *Journal of Aircraft*, Vol. 44, No. 5, pp. 1610–1618, 2008.
[11] M. K. Singha and Mukul Mandal, "Supersonic flutter characteristics of composite cylindrical panel", *Composite Structures*, Vol. 82, pp. 295-301, 2008.
[12] H. Haddadpour, S. Mahmoudkhani, and H. M. Navazi, "Supersonic Flutter Prediction of Functionally Graded Cylindrical Shells", *Composite Structures*, Vol. 83, pp. 391-398, 2008.
[13] V. Birman, "Review Of Mechanics of Shape Memory Alloy Structures", *Appl. Mech. Rev.*, Vol. 50, pp. 629-645, 1997.
[14] H. S. Lee, J. J. Lee, and J. S. Huh, "A Simulation Study on the Thermal Buckling Behavior of Laminated Composite Shells with Embedded Shape Memory Alloy (SMA) Wires", *Composite Structures*, Vol. 47, pp. 463-469, 1999.
[15] M. Tawfik, J. J. Ro, and C. Mei, "Thermal Post-Buckling and Aeroelastic Behavior of Shape Memory Alloy Reinforced Plates", *Smart Materials and Structures*, Vol. 11, 297-307, 2002.
[16] J. S. Park, J. H. Kim, and S. H. Moon, "Vibration of Thermally Post-Buckled Composite Plates Embedded With Shape Memory Alloy Fibers", *Composite Structures*, Vol. 63, pp. 179-188, 2004.
[17] J. H. Roh, I. K. Oh, S. M. Yang, J. H. Han and I. Lee, "Thermal Post-Buckling Analysis of Shape Memory Alloy Hybrid Composite Shell Panels", *Smart Materials and Structures*, Vol. 13, pp. 1337-1344, 2004.
[18] H. H. Ibrahim, M. Tawfik, and H. M. Negm, "Thermal Postbuckling and Flutter Behavior of Shape Memory Alloy Hybrid Composite Plates," Proceedings of the *8th International Congress of Fluid Dynamics and Propulsion (ICFDP 8)*, *ASME* Paper ICFDP-EG-153, 2006.
[19] H. H. Ibrahim, M. Tawfik, and H. M. Negm, "Thermo-acoustic Random Response of Shape Memory Alloy Hybrid Composite Plates," *Journal of Aircraft*, in press, DOI: 10.2514/1.32843.
[20] H. H. Ibrahim, M. Tawfik, H. H. Yoo, and K. S. Lee, "Aero-Thermo-Mechanical Characteristics of Shape Memory Alloy Hybrid Composite Panels with Initial Geometric Imperfection", Proceedings of the *15th International Congress on Sound and Vibration(ICSV15)*, Daejeon, South Korea, 2008.
[21] M. S. Azzouz, "Nonlinear Flutter of Curved Panels Under Yawed Supersonic Flow Using Finite Elements", PhD Dissertation, *Old Dominion University, Mechanical Engineering Department*, Norfolk, Virginia, 2005.
[22] W. B. Cross, A. H. Kariotis, and F. j. Stimeler, "Nitinol Characterization Study", *NASA CR-14B*, 1969.